

1            Quantitative Analysis of Powder Mixtures by  
2 Raman Spectrometry: the influence of particle size  
3            and its correction  
4  
5

6 Zeng-Ping Chen<sup>\*a</sup>, Li-Mei Li<sup>a</sup>, Jing-Wen Jin<sup>a</sup>, Alison Nordon<sup>b</sup>, David Littlejohn<sup>b</sup>, Jing Yang<sup>a</sup>,  
7            Juan Zhang<sup>a</sup>, Ru-Qin Yu<sup>a</sup>  
8  
9  
10

11        *a. State Key Laboratory of Chemo/Biosensing and Chemometrics, College of Chemistry and*  
12            *Chemical Engineering, Hunan University, Changsha 410082, China*

13        *b. WestCHEM, Department of Pure and Applied Chemistry and Centre for Process Analytics*  
14            *and Control Technology, University of Strathclyde, Glasgow, G1 1XL, Scotland, UK*  
15  
16  
17

18        *\* Corresponding author*

19        Tel.: (+86) 731 88821916; Fax: (+86) 731 88821916;

20        E-Mail Address: [zpchen2002@hotmail.com](mailto:zpchen2002@hotmail.com) (Z.P. Chen)  
21

22 **Abstract:** Particle size distribution and compactness have significant confounding effects on  
23 Raman signals of powder mixtures, which cannot be effectively modeled or corrected by  
24 traditional multivariate linear calibration methods such as partial least squares (PLS), and  
25 therefore greatly deteriorate the predictive abilities of Raman calibration models for powder  
26 mixtures. The ability to obtain directly quantitative information from Raman signals of  
27 powder mixtures with varying particle size distribution and compactness is, therefore, of  
28 considerable interest. In this study, an advanced quantitative Raman calibration model was  
29 developed to explicitly account for the confounding effects of particle size distribution and  
30 compactness on Raman signals of powder mixtures. Under the theoretical guidance of the  
31 proposed Raman calibration model, an advanced dual calibration strategy was adopted to  
32 separate the Raman contributions caused by the changes in mass fractions of the constituents  
33 in powder mixtures from those induced by the variations in the physical properties of samples,  
34 and hence achieve accurate quantitative determination for powder mixture samples. The  
35 proposed Raman calibration model was applied to the quantitative analysis of backscatter  
36 Raman measurements of a proof-of-concept model system of powder mixtures consisting of  
37 barium nitrate and potassium chromate. The average relative prediction error of prediction  
38 obtained by the proposed Raman calibration model was less than one-third of the  
39 corresponding value of the best performing PLS model for mass fractions of barium nitrate in  
40 powder mixtures with variations in particle size distribution as well as compactness.

41 **Keywords:** Quantitative Raman Spectroscopic Analysis, Particle Size Distribution,  
42 Compactness, Multiplicative Confounding Effects, Powder Mixture, Dual Calibration  
43 Strategy

## 44 **Introduction**

45 Powder blending is an important process in the manufacture of many pharmaceutical  
46 products<sup>1</sup>. Raman spectroscopy has been increasingly applied to the qualitative analysis of  
47 powder mixtures<sup>2-6</sup>, because of its flexibility of sampling (solids can be analyzed with little  
48 or no sample preparation), and exceptionally high chemical specificity and the use of fibre  
49 optics for convenient and remote analysis, which facilitate the non-invasive in-line and real  
50 time analysis of particulate systems<sup>7-17</sup>. However, some issues remain unresolved regarding  
51 the quantitative in-line monitoring of particulate systems by Raman spectroscopy.

52 One of the issues is that the Raman intensities of analyte peaks depend on not only the  
53 analyte concentration, but also on the intensity of the excitation source, the instrument's  
54 optical configuration and the sample alignment. Therefore, to gain quantitative information  
55 requires the use of internal or external standards<sup>18-20</sup>. Band ratios between the overall Raman  
56 intensities and that of an individual spectral peak arising from internal or external standards  
57 are calculated and used in quantitative analysis. But the use of internal or external standards  
58 can be difficult to apply accurately in many *in-situ* process analysis applications. Moreover,  
59 for samples involving solids such as powder mixtures, quantitative Raman analysis becomes  
60 even more difficult, because the Raman measurements from such samples depend on the  
61 particle size and compactness of the mixtures, which hinders the use of an internal or external  
62 standard. The application of multivariate calibration methods such as principal component  
63 regression (PCR) and partial least squares (PLS) has some advantages over univariate band  
64 ratio calibration models in the quantitative analysis of Raman measurements<sup>20,21</sup>. However,  
65 when analyzing powder mixtures using Raman spectroscopy, the variations in the physical

66 properties such as particle size and compactness of the mixtures have confounding effects on  
67 the total Raman intensities. Such confounding effects cannot be effectively modeled by  
68 standard multivariate calibration methods, and will significantly affect the predictive  
69 accuracy of multivariate calibration models.

70 Although it has long been known that physical properties of powder samples can  
71 influence the intensity of the Raman spectrum, and several studies<sup>22-26</sup> have been conducted  
72 on the relationship between particle size and Raman intensity, relatively little research  
73 focuses on quantitative Raman spectroscopic analysis of powder mixtures. Some of the  
74 present authors conducted a preliminary investigation on quantitative Raman spectroscopic  
75 analysis of suspension samples<sup>27</sup>. However, due to the facility limitations at that time, we  
76 were unable to explicitly investigate the effects of particle size distribution and sample  
77 compactness on Raman signals of powder mixtures in that work. The objectives of this study  
78 are to 1) explicitly investigate the effects of particle size and compactness on Raman signals  
79 of powder mixtures, 2) develop an advanced quantitative Raman calibration model for  
80 powder mixtures, and 3) eventually achieve accurate quantitative analysis of powder mixtures  
81 using Raman spectrometry.

82

83

## 84 **Theory**

### 85 *Raman intensities of powder mixtures*

86 The intensity of Raman bands depends on a complex expression involving the polarisability  
87 tensor of a molecule<sup>28</sup>. For analytical purposes, the following less rigorous linear model

88 analogous to the Beer-Lambert law can be used.

$$I(\nu) = n \cdot r(\nu) \cdot I_o \quad (1)$$

89 Where  $I(\nu)$  is the Raman intensity at Raman shift  $\nu$ ,  $I_o$  is the intensity of the excitation  
90 radiation,  $n$  is the number of molecules of the analyte illuminated by the source and viewed  
91 by the spectrometer, and  $r(\nu)$  is a composite term that represents the overall spectrometer  
92 response, and the self absorption and molecular scattering properties of the analyte at Raman  
93 shift  $\nu$ . For  $K$  powder samples comprising  $J$  constituents with amounts above their Raman  
94 limits of detection, their overall Raman intensities can be expressed as the linear combination  
95 of the contributions of all  $J$  constituents as well as other possible interference(s) such as  
96 fluorescence.

$$I_k(\nu) = \sum_{j=1}^J [n_{k,j} \cdot r_j(\nu) \cdot I_{o,k}] + n_{k,interf} \cdot r_{interf}(\nu) \cdot I_{o,k}; \quad k = 1, 2, \dots, K \quad (2)$$

97 Where  $n_{k,j}$  and  $n_{k,interf}$  are the number of molecules of the  $j$ -th constituent and the  
98 interference(s) in the  $k$ -th powder sample illuminated by the source and viewed by the  
99 spectrometer, respectively;  $r_{interf}(\nu)$  represents the molecular scattering/fluorescence  
100 properties of the interference(s) at Raman shift  $\nu$ .

101 Suppose  $m_k$  and  $V_k$  are the overall mass and volume of the  $k$ -th powder sample,  
102 respectively.  $V_{spec,k}$  denotes the volume of the  $k$ -th powder sample illuminated by the source  
103 and viewed by the spectrometer.  $w_{k,j}$  ( $\sum_{j=1}^J w_{k,j} = 1$ ) signifies the mass fraction of the  $j$ -th  
104 constituent in the  $k$ -th sample.  $M_j$  is the molecular weight of the  $j$ -th constituent. The  
105 multiplicative parameter,  $p_k$ , is introduced to account for the effects of the particle size

106 distribution and compactness of the  $k$ -th sample on the Raman intensities<sup>24, 27</sup>. Equation 2  
 107 then becomes:

$$I_k(\nu) = \sum_{j=1}^J [p_k \cdot \frac{m_k \cdot w_{k,j} \cdot V_{spec,k}}{M_j \cdot V_k} \cdot r_j(\nu) \cdot I_{o,k}] + n_{k,interf} \cdot r_{interf}(\nu) \cdot I_{o,k} \quad (3)$$

108 Define  $q_k = p_k \cdot m_k \cdot V_{spec,k} \cdot I_{o,k} / V_k$  and  $r_j^*(\nu) = r_j(\nu) / M_j$ . Equation 3 can be simplified as  
 109 follows.

$$I_k(\nu) = \sum_{j=1}^J [q_k \cdot w_{k,j} \cdot r_j^*(\nu)] + n_{k,interf} \cdot r_{interf}(\nu) \cdot I_{o,k} \quad (4)$$

110 In equation 4,  $q_k$  is a very important model parameter. It accounts for the variations in Raman  
 111 intensities caused by the changes in variables other than the mass fractions of the constituents  
 112 in the powder mixtures, such as the intensity of the excitation source, the sample's particle  
 113 size distribution, sample compactness, the overall mass and volume of the powder sample as  
 114 well as the volume illuminated by the source and viewed by the spectrometer.

115 Suppose the  $j$ -th constituent is the target component in the powder mixtures, and the  
 116 Raman signals of  $K$  calibration samples have been measured over Raman shift range of  $\nu_1 \sim \nu_m$ .

117 As  $\sum_{j=1}^J w_{k,j} = 1$ , equation 4 can be rewritten as:

$$\mathbf{x}_k = q_k \cdot w_{k,1} \cdot \Delta \mathbf{r}_1^* + q_k \cdot \mathbf{r}_2^* + \sum_{j=3}^J [q_k \cdot w_{k,j} \cdot \Delta \mathbf{r}_j^*] + n_{k,interf} \cdot \mathbf{r}_{interf} \cdot I_{o,k} \quad (5)$$

Where,  $\mathbf{x}_k = [I_k(\nu_1), I_k(\nu_2), \dots, I_k(\nu_m)]$ ;  $\mathbf{r}_j^* = [r_j^*(\nu_1), r_j^*(\nu_2), \dots, r_j^*(\nu_m)]$ ,  $j = 1, 2, \dots, J$

$$\Delta \mathbf{r}_j^* = \mathbf{r}_j^* - \mathbf{r}_2^*; \quad \mathbf{r}_{interf} = [r_{interf}(\nu_1), r_{interf}(\nu_2), \dots, r_{interf}(\nu_m)]$$

118 Assuming  $\Delta \mathbf{r}_j^*$ ,  $\mathbf{r}_2^*$ , and  $\mathbf{r}_{interf}$  are linearly independent of each other, it can be seen that a  
 119 straightforward multivariate linear calibration model can be built only between  $\mathbf{x}_k$  and  
 120  $q_k \cdot w_{k,j}$  (or  $q_k$ ). It is obvious that the multiplicative parameter,  $q_k$ , may be different for each

121 of the powder samples. Hence the relationship between Raman spectrum  $\mathbf{x}_k$  and the mass  
 122 fraction of the  $j$ -th constituent ( $w_{k,j}$ ) is actually nonlinear; and the multiplicative parameter,  $q_k$ ,  
 123 has confounding effects on the estimation of  $w_{k,j}$ . In order to extract the quantitative  
 124 information (mass fraction) of any constituent in powder samples from their Raman  
 125 measurements, it is therefore imperative to estimate the multiplicative parameter,  $q_k$ , for each  
 126 powder sample.

127

128 *Dual Calibration Strategy (DCS)*<sup>27, 29-30</sup>

129 For  $K$  training samples in which the mass fractions of the target constituent (say, the  $j$ -th  
 130 constituent) are known, the multiplicative parameters,  $q_k$  ( $k = 1, 2, \dots, K$ ), can be estimated by  
 131 the modified Optical Path-Length Estimation and Correction method (OPLEC<sub>m</sub>)<sup>30</sup> ( the  
 132 Matlab script for OPLEC<sub>m</sub> is provided in supporting information). After the estimation of  $q_k$   
 133 ( $k = 1, 2, \dots, K$ ), the following two calibration models can be built by multivariate linear  
 134 calibration methods such as PLS.

$$\begin{aligned} \text{diag}(\mathbf{w}_j)\mathbf{q} &= a_1\mathbf{1} + \mathbf{X}_{cal}\boldsymbol{\beta}_1; \quad \mathbf{q} = a_2\mathbf{1} + \mathbf{X}_{cal}\boldsymbol{\beta}_2 \\ \mathbf{X}_{cal} &= [\mathbf{x}_1; \mathbf{x}_2; \dots; \mathbf{x}_K]; \quad \mathbf{w}_j = [w_{1,j}; w_{2,j}; \dots; w_{K,j}]; \quad \mathbf{q} = [q_1; q_2; \dots; q_K] \end{aligned} \quad (6)$$

135 Where  $\text{diag}(\mathbf{w}_j)$  denotes the diagonal matrix in which the corresponding diagonal elements are  
 136 the elements of  $\mathbf{w}_j$ ;  $\mathbf{1}$  is a column vector with its elements equal to unity. After the estimation  
 137 of model parameters  $a_1$ ,  $a_2$ ,  $\boldsymbol{\beta}_1$ , and  $\boldsymbol{\beta}_2$  by multivariate calibration methods such as PLS,  
 138 these two calibration models could then be used to predict the mass fraction of the target  
 139 constituent in any test powder sample ( $w_{test,j}$ ) from its Raman spectrum  $\mathbf{x}_{test}$ .

$$q_{test} \cdot w_{test,j} = a_1 + \mathbf{x}_{test} \boldsymbol{\beta}_1; \quad q_{test} = a_2 + \mathbf{x}_{test} \boldsymbol{\beta}_2; \quad w_{test,j} = \frac{a_1 + \mathbf{x}_{test} \boldsymbol{\beta}_1}{a_2 + \mathbf{x}_{test} \boldsymbol{\beta}_2} \quad (7)$$

140 The mass fraction of other constituents in the test sample can be obtained in a similar way.

141

142

## 143 **Experimental**

### 144 *Materials*

145 All chemicals were analytical grade, and were used as received without any further  
 146 purification. Potassium chromate was obtained from Tianjin Windship Chemistry  
 147 Technological Co., Ltd (Tianjin, China). Barium nitrate was purchased from Tianjin Kermel  
 148 Chemical Reagent Co., Ltd (Tianjin, China).

149

### 150 *Equipment*

151 Raman spectra were acquired at room temperature on a LABRAM-0101 Laser Confocal  
 152 Raman Spectrometer equipped with a 1024×256 pixels CCD detector. The microscope  
 153 attachment was based on an Olympus BX41 system with a 10× objective. Radiation of  
 154 632.81 nm from a 17 mW He-Ne laser was used for excitation. The widths of the entrance slit  
 155 and confocal pinhole were set to 100 μm and 1000 μm, respectively. Raman spectrum  
 156 between 200 and 2000 cm<sup>-1</sup> was collected with a 5 s exposure time and 3 accumulations for  
 157 each spectrum.

158

### 159 *Raman measurements of powder mixtures*

160 The solids of both barium nitrate and potassium chromate were ground and sorted into



161 different particle sizes using standard sieves. The standard sieves were of mesh sizes 40, 60,  
162 80, 100, 120, 140, 160 and 200 wires per inch. The hole sizes corresponding to the mesh sizes  
163 are 425, 250, 180, 150, 125, 109, 96 and 75  $\mu\text{m}$ , respectively. A total of 72 powder mixtures  
164 of potassium chromate and barium nitrate powder with different weight ratios (1:0, 0.90:0.10,  
165 0.75:0.25, 0.60:0.40, 0.50:0.50, 0.40:0.60, 0.25:0.75, 0.10:0.90 and 0:1) and different particle  
166 sizes (425, 250, 180, 150, 125, 109, 96 and 75  $\mu\text{m}$ ) were prepared by mixing appropriate  
167 amounts of the two constituents thoroughly (Table 1). For each of 72 powder mixtures, a  
168 sample was randomly taken and loosely packed into a cylindrical sample cup with a diameter  
169 of 6.9 mm and a height of 10.7 mm. The laser beam was focused at a point inside the sample  
170 so as to ensure the illumination of the whole upper surface of the sample by the laser beam,  
171 and then the Raman spectrum was acquired. Following this, each sample was packed more  
172 firmly, and a further Raman spectrum was recorded resulting in a total of 144 spectra.  
173 Seventy eight spectra (two outliers were removed) from the five mixtures with the ratios of  
174 potassium chromate to barium nitrate equal to 1:0, 0.75:0.25, 0.5:0.5, 0.25:0.75 and 0:1  
175 formed the calibration data set. The test set comprised the remaining 64 spectra from the  
176 other four mixtures. Distinctive Raman peaks of potassium chromate (at around 351, 386.5,  
177 396.8, 853.4, 868.4, 877.8 and 906.8  $\text{cm}^{-1}$ ) and barium nitrate (at about 1047.5  $\text{cm}^{-1}$ ) can be  
178 readily observed between 292.8 and 1136.6  $\text{cm}^{-1}$  (supporting information, Figure S-1).  
179 Therefore, Raman signals in this region were selected for the subsequent data analysis.

180 Table 1: Mass ratios and particle sizes of potassium chromate and barium nitrate in powder mixtures.

181

Sample No.	K <sub>2</sub> CrO <sub>4</sub> /Ba(NO <sub>3</sub> ) <sub>2</sub> (mass ratio)	Particle Size (μm)
1 – 8	1:0	425, 250, 180, 150, 125, 109, 96, 75
9 – 16	0.90:0.10	425, 250, 180, 150, 125, 109, 96, 75
17 – 24	0.75:0.25	425, 250, 180, 150, 125, 109, 96, 75
25 – 32	0.60:0.40	425, 250, 180, 150, 125, 109, 96, 75
33 – 40	0.50:0.50	425, 250, 180, 150, 125, 109, 96, 75
41 – 48	0.40:0.60	425, 250, 180, 150, 125, 109, 96, 75
49 – 56	0.25:0.75	425, 250, 180, 150, 125, 109, 96, 75
57 – 64	0.10:0.90	425, 250, 180, 150, 125, 109, 96, 75
65 – 72	0:1	425, 250, 180, 150, 125, 109, 96, 75

182

183

184

185

186

187

188

189

190

191 *Data analysis*

192 Due to the influence of particle size and compactness on Raman intensities, it is unlikely that  
193 univariate analysis will give accurate predictions of the mass fractions of barium nitrate in  
194 powder mixtures. Therefore, PLS and the dual calibration strategy (DCS) were adopted for  
195 the data analysis and their performance in terms of providing accurate predictions for the  
196 mass fractions of barium nitrate in powder mixtures were compared. The effectiveness of  
197 multiplicative signal correction (MSC)<sup>31</sup>, standard normal variate (SNV)<sup>32</sup> and extended  
198 inverted signal correction (EISC)<sup>33</sup> in correcting the confounding effects of physical  
199 properties of powder samples on the Raman measurements and improving the predictive  
200 abilities of PLS calibration models were also investigated. For the convenience of  
201 presentation, PLS calibration models built on the mean-centred raw and preprocessed Raman  
202 spectra by MSC, EISC and SNV are denoted by PLS\_raw, PLS\_MSC, PLS\_EISC and  
203 PLS\_SNV, respectively. No pre-processing methods other than mean-centring were used  
204 when building DCS calibration models. The optimal calibration models were selected  
205 through a cross-validation procedure. During cross-validation, the Raman spectra of the  
206 calibration samples with the same mass ratio of potassium chromate to barium nitrate were  
207 left out in turn and the root mean square error of prediction from cross validation (RMSEP<sub>cv</sub>)  
208 values were calculated. The calibration models with the minimal RMSEP<sub>cv</sub> values were  
209 taken as the optimal models, and were then used to predict the mass fractions of barium  
210 nitrate in the test samples. The data analysis was performed on a Pentium class computer  
211 using Matlab version 6.5 (Mathworks, Inc). All the programmes including DCS, PLS, MSC,  
212 SNV, and EISC were written in house.

213

214 **Results and discussion**

215 *The sensitivity of Raman intensities to the mass fraction of barium nitrate*

216 Figure 1a shows the Raman spectra of powder mixtures samples with the same particle size  
217 (250  $\mu\text{m}$ ) and similar compactness but different mass ratios of potassium chromate to barium  
218 nitrate. The Raman peaks are relatively sensitive to the changes in the composition of the  
219 powder mixtures. The Raman peak intensity at  $1047.5\text{ cm}^{-1}$  generally increases with mass  
220 fraction of barium nitrate in the powder samples. However, the relationship between Raman  
221 peak intensity and mass fraction of barium nitrate deviates from a perfect linear model even  
222 when samples have a similar particle size and degree of compactness (Figure 1b). Especially  
223 there is a discontinuity which might be caused by the variation in excitation intensity or  
224 packing density. This demonstrates the necessity to introduce the multiplicative parameter,  $q_k$ ,  
225 in eq.4 to account for the variations in Raman intensities caused by the changes in variables  
226 other than the mass fractions of the constituents in the powder mixtures.

227

228

229

230

231

232

233

234

235

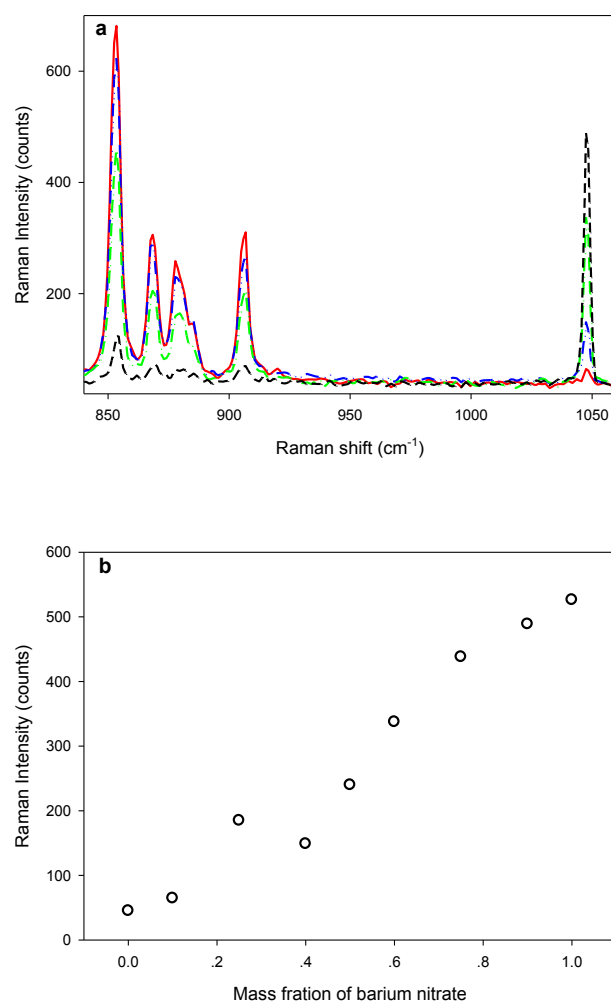


Figure 1: a) Raman spectra of loosely packed powder mixture samples (particle size: 250  $\mu\text{m}$ ) with different mass ratios of potassium chromate to barium nitrate (red solid line: 0.9:0.1; blue dash-dot-dot line: 0.6:0.4; green dash-dot line: 0.4:0.6; black dash line: 0.1:0.9); b) Raman peak intensity at 1047.5  $\text{cm}^{-1}$  vs mass fraction of barium nitrate in loosely packed powder mixture samples (particle size: 250  $\mu\text{m}$ ).

237 *The effects of particle size and compactness on Raman intensities*

238 In addition to the mass ratio of potassium chromate to barium nitrate, the particle size and  
239 compactness of the powder mixture samples also have a significant influence on the Raman  
240 peak intensities. As shown in Figure 2a, a firmly packed sample has significantly more  
241 intense Raman peaks than those of a loosely packed sample with the same mass ratio and  
242 particle size. It has long been known that particle size differences make significant  
243 contributions to the spectral variations in Raman measurements of powders<sup>22</sup>. Our  
244 experimental results also show that variations in particle size of powder samples have  
245 significant effects on the Raman spectra (Figure 2b). For two samples with the same particle  
246 size (109  $\mu\text{m}$ ) but different mass ratios of potassium chromate to barium nitrate (e.g.  
247 0.25:0.75 and 0.10:0.90), the difference between the peak intensities at 1047.5  $\text{cm}^{-1}$  is 59.04.  
248 While for two samples with the same mass ratio of potassium chromate to barium nitrate  
249 (0.10:0.90) but different particle sizes (e.g. 109 and 75  $\mu\text{m}$ ), the difference between the  
250 corresponding peak intensities is 113.63, which is about 1.9 times that caused by a change in  
251 the mass ratio of potassium chromate to barium nitrate from 0.25:0.75 to 0.90:0.10. Moreover,  
252 variation in the particle size of a sample has the same effect on all Raman peaks in the  
253 spectrum. This makes it difficult to discriminate Raman intensity contributions caused by  
254 changes in a sample's particle size from those due to a variation in mass fractions of the  
255 chemical constituents using traditional univariate/multivariate calibration methods. If not  
256 properly modelled, this difference would significantly degrade the accuracy and reliability of  
257 calibration models built on Raman measurements contaminated by such confounding effects.  
258 The multiplicative parameter,  $q_k$ , in eq.4 accounts for the effects of particle size and

259 compactness on the Raman intensities and so their effects can be separated from those of the  
260 mass fractions of the chemical constituents in powder samples by the unique dual calibration  
261 strategy.

262

263

264

265

266

267

268

269

270

271

272

273

274

275

276

277

278

279

280

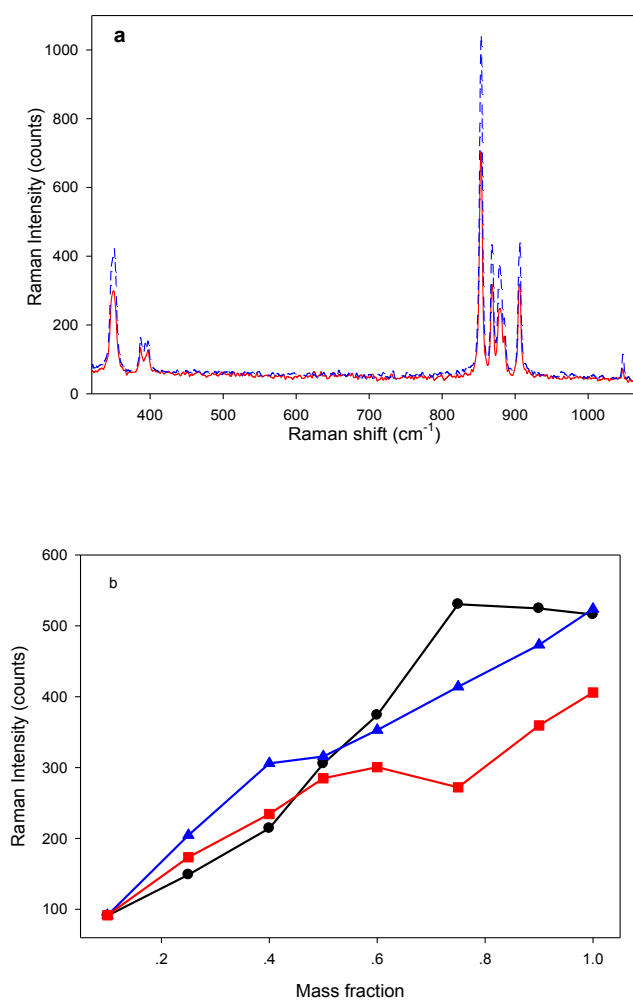


Figure 2: a) Raman spectra of a binary powder mixture sample (potassium chromate:barium nitrate: 0.90:0.10, particle size: 425  $\mu\text{m}$ ) with different compactness (blue dash line: firmly packed; red solid line: loosely packed); b) peak intensity at 1047.5  $\text{cm}^{-1}$  vs mass fraction of barium nitrate with different particle sizes (black circle: 180  $\mu\text{m}$ ; blue triangle: 109  $\mu\text{m}$ ; red square: 75  $\mu\text{m}$ ).



282 *Correction of the multiplicative effects of particle size and compactness on Raman intensities*

283 As shown in the preceding section, the presence of significant multiplicative confounding  
284 effects (arising from differences in particle size and compactness) caused deviations in the  
285 linear relationship between the Raman intensities and the mass fraction of solid powder  
286 samples. With a view to mitigate the influence of the multiplicative confounding effects  
287 present in the Raman spectral data, the dual calibration strategy (DCS) was employed to  
288 correct such confounding effects. For the purpose of comparison, PLS models with and  
289 without the use of pre-processing methods MSC, EISC and SNV were also applied to the  
290 same Raman spectral data. DCS involves the estimation of the multiplicative parameter,  $q_k$ ,  
291 for each calibration sample by OPLEC<sub>m</sub><sup>30</sup>. The implementation of OPLEC<sub>m</sub> requires the  
292 determination of the number of spectral variation sources including chemical components and  
293 possible interference(s). For the powder mixture samples studied in this paper, the number of  
294 spectral variation sources is two, i.e. potassium chromate and barium nitrate. The results of  
295 OPLEC<sub>m</sub> are shown in Figure 3. It is evident that different calibration samples generally have  
296 different multiplicative parameter values ( $q_k$ ) and the multiplicative parameter,  $q_k$ , of the  
297 calibration samples varies in the range of 1 – 2.23. These results demonstrate that the  
298 presence of significant multiplicative confounding effects in the Raman spectral data and the  
299 introduction of the multiplicative parameter,  $q_k$ , in eq.4 is theoretically sound and also  
300 practically relevant. Otherwise, the multiplicative parameter values ( $q_k$ ) calculated by  
301 OPLEC<sub>m</sub> for the calibration samples would vary within a narrow range, and would also be  
302 quite close to 1.

303

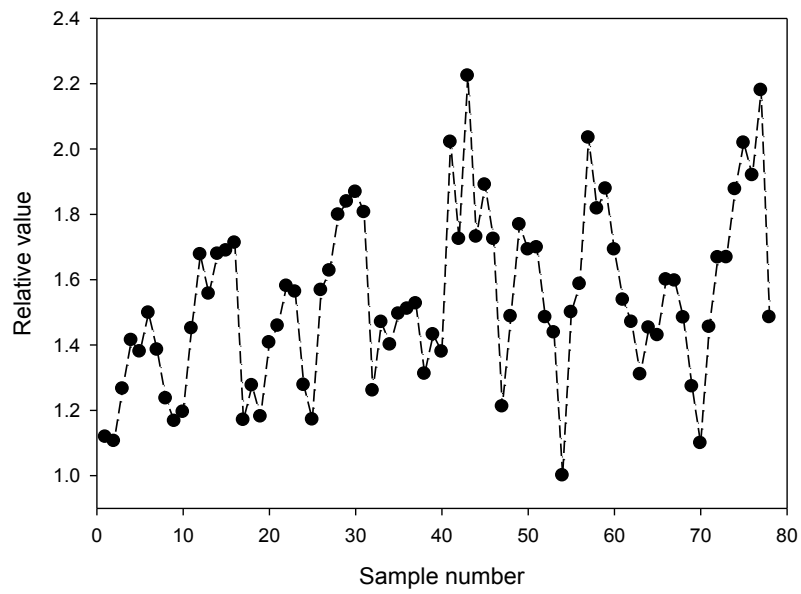


Figure 3: the multiplicative parameter  $q_k$  for the calibration samples estimated by  $OPLEC_m$ .

304

305

306

307

308

309

310

311

312

313

314

315 After the calculation of the multiplicative parameters,  $q_k$ , for each calibration sample by  
316 OPLEC<sub>m</sub>, DCS models with different underlying components were built. Values of the root  
317 mean square error of prediction from cross validation (RMSEP<sub>cv</sub>) obtained by DCS and the  
318 various PLS calibration models (i.e. PLS<sub>raw</sub>, PLS<sub>MSC</sub>, PLS<sub>EISC</sub> and PLS<sub>SNV</sub>) with  
319 different number of latent variables are given in supporting information, Figure S-2. Both the  
320 PLS<sub>raw</sub> and PLS<sub>MSC</sub> models attained minimum RMSEP<sub>cv</sub> values of 0.08 and 0.12,  
321 respectively, when two latent variables were used. For PLS<sub>EISC</sub> and PLS<sub>SNV</sub>, only one  
322 latent variable was suggested by cross validation; however, the RMSEP<sub>cv</sub> values of 0.26 and  
323 0.23, respectively, were significantly larger than that for PLS<sub>raw</sub>, which to some extent  
324 indicates the inappropriateness of applying EISC and SNV to this particular Raman spectral  
325 data set. In contrast with the above PLS calibration models, a DCS model with three latent  
326 variables had a minimum RMSEP<sub>cv</sub> value of 0.03, which is less than half that of the  
327 corresponding value obtained with the PLS<sub>raw</sub> model.

328 For a more convincing comparison, the performance of the optimal DCS and various  
329 PLS calibration models for the independent test samples was investigated. As shown in  
330 Figure 4 and Figure 5, the RMSEP value of the optimal PLS<sub>raw</sub> model obtained for the  
331 independent test samples was 0.08 (equivalent to a mean relative prediction error of 30.8%),  
332 which clearly demonstrates the presence of detrimental multiplicative confounding effects  
333 caused by variations in the particle size and compactness of powder samples. The application  
334 of MSC, EISC and SNV resulted in a deterioration of the predictive ability of the PLS  
335 calibration models. This confirms that the pre-processing methods MSC, EISC and SNV  
336 cannot effectively correct the multiplicative confounding effects of particle size and

337 compactness on Raman intensities. In contrast, the optimal DCS model with 3 latent variables  
338 achieved a RMSEP value of 0.04 for the independent test samples, which is equivalent to a  
339 mean relative prediction error of 9.6%, less than one third of the corresponding value for the  
340 optimal PLS\_raw model. Even more interestingly, though the construction of the DCS model  
341 requires no extra information or data compared to the PLS models, it consistently  
342 outperformed the various PLS models built on the raw and pre-processed Raman spectra, no  
343 matter how many latent variables were used (Figure S-3 in supporting information). The  
344 significant reduction in the RMSEP value achieved with the optimal DCS model results  
345 solely from the introduction of the multiplicative parameter,  $q_k$ , in eq. 4 to account for the  
346 variations in Raman intensities caused by the changes in variables other than the mass  
347 fractions of the chemical constituents in powder mixtures, in this case particle size and  
348 compactness.

349

350

351

352

353

354

355

356

357

358

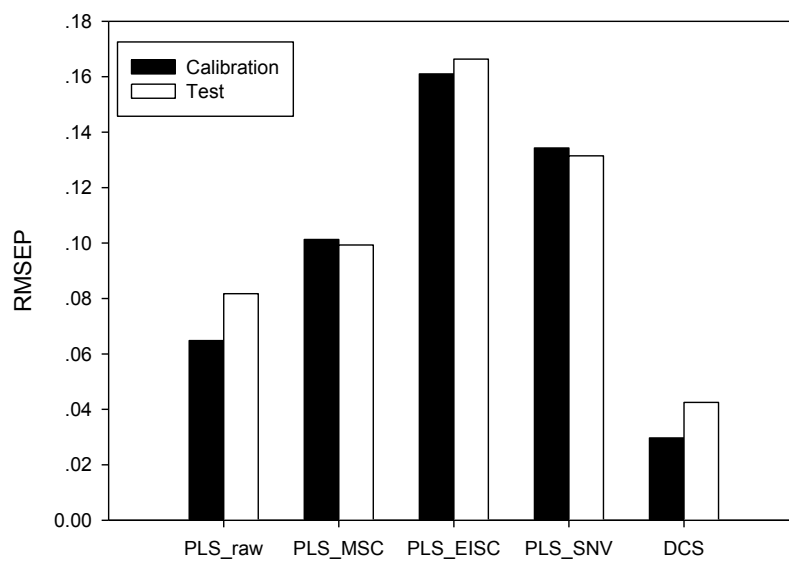


Figure 4: the RMSEP values for both the calibration and independent test samples obtained by different calibration methods.

360

361

362

363

364

365

366

367

368

369

370

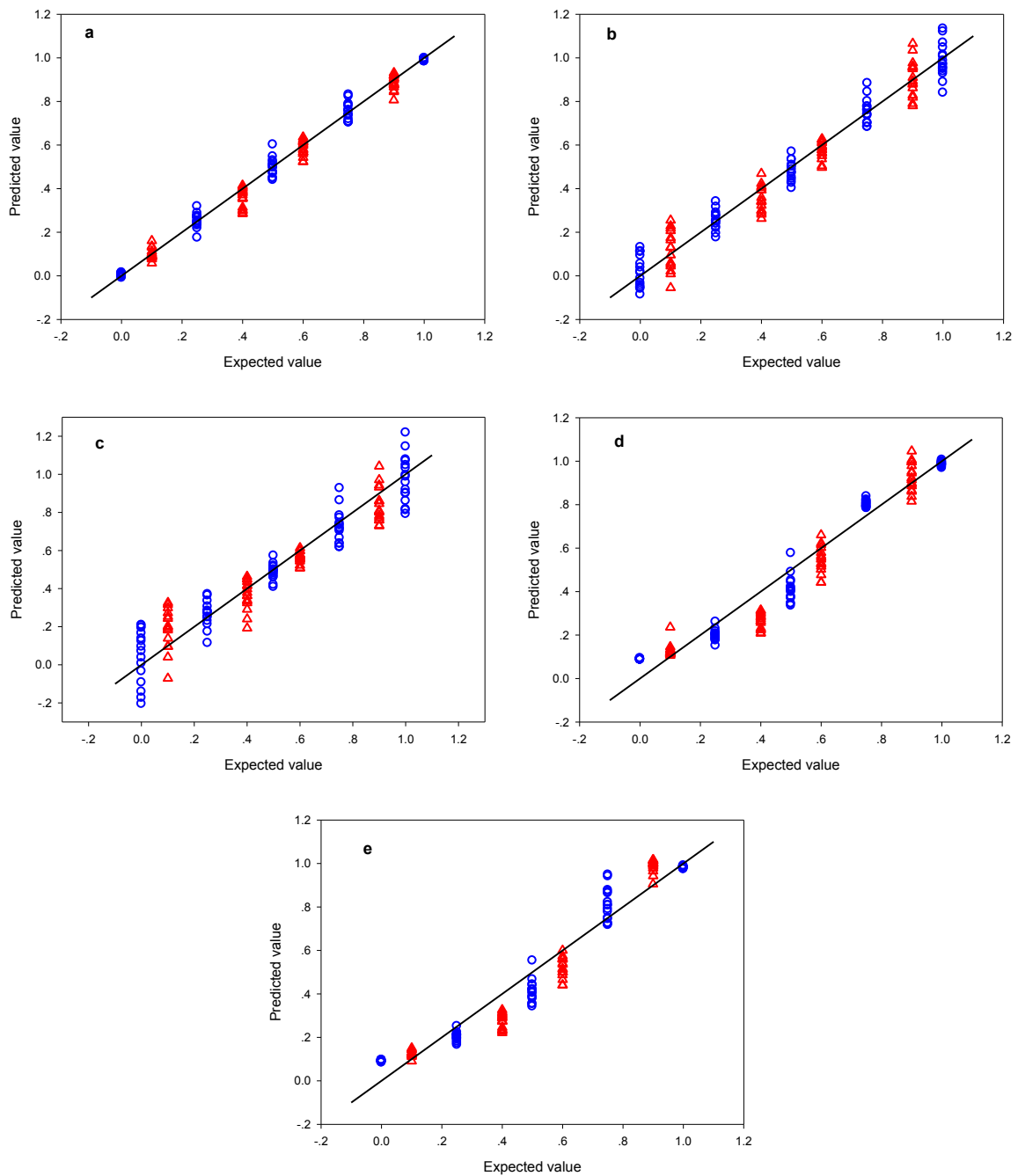


Figure 5: the mass fractions of  $\text{Ba}(\text{NO}_3)_2$  in the calibration (blue circle) and independent test (red triangle) samples predicted by various calibration models (a: DCS; b: PLS\_raw; c: PLS\_MSC; d: PLS\_SNV; e: PLS\_EISC)

372 **Conclusions**

373 The Raman intensities of powder mixture samples depend on not only the mass fractions of  
374 the chemical constituents but also the physical properties of samples such as particle size  
375 distribution and compactness. The experimental results on a model system of powder  
376 mixtures consisting of barium nitrate and potassium chromate showed that the effects of  
377 particle size distribution and compactness on Raman measurements are multiplicative, which  
378 cannot be effectively modelled by multivariate linear calibration methods such as PLS.  
379 Pre-processing the Raman measurements with multiplicative confounding effects of particle  
380 size and compactness by MSC, SNV or EISC could not improve but rather deteriorated the  
381 predictive performance of Raman calibration models. In this work, we introduced a  
382 multiplicative parameter in the quantitative Raman calibration model to explicitly account for  
383 the confounding effects of particle size and compactness on Raman signals of powder  
384 mixtures, and then eliminated the confounding effects through a unique dual calibration  
385 strategy. The average relative prediction error of predictions obtained by the dual calibration  
386 strategy for the independent test samples was less than one-third of the corresponding value  
387 of the optimal PLS calibration models built using the raw Raman spectra and considerably  
388 better than the results of PLS models based on spectra pre-processed by application of MSC,  
389 EISC or SNV. These results demonstrate that the dual calibration strategy can effectively  
390 mitigate the confounding effects of samples' physical properties and so improve the accuracy  
391 of quantitative analysis of powders using Raman spectrometry. Hence, the dual calibration  
392 strategy will be of major benefit for quantitative measurement of particulate samples such as  
393 powder blends and pharmaceutical dosage forms.

394

395 **Acknowledgements**

396 The authors acknowledge the financial support of the National Natural Science Foundation of  
397 China (grant no. 21075034 and grant no. 21035001) and the National Instrumentation  
398 Program of China (grant no. 2011YQ0301240102). AN acknowledges the award of a  
399 University Research Fellowship by the Royal Society, UK.

400

401

402 **Supporting Information Available**

403 MATLAB code for the modified OPLEC method, Raman spectra of  $K_2CrO_4$  and  $Ba(NO_3)_2$ ;  
404 The RMSEP values from cross validation obtained by DCS and various PLS calibration  
405 models with different number of latent variables built on the raw and pre-processed Raman  
406 spectra by MSC, SNV, and EISC; The RMSEP values for the test powder mixtures obtained  
407 by DCS and various PLS calibration models with different number of latent variables built on  
408 the raw and pre-processed Raman spectra by MSC, SNV, and EISC. This material is  
409 available free of charge via the Internet at <http://pubs.acs.org>.

410

411

412

413

414

415

416



417 **References:**

- 418 [1]. Berman, J. *PDA J. Pharm. Sci. Tech.* **2001**, *55*, 209-222
- 419 [2]. De Beer, T.R.M.; Bodson, C.; Dejaegher, B.; Walczak, B.; Vercruyssen, P.; Burggraeve,  
420 A.; Lemos, A.; Delattre, L.; Varder Herden, Y.; Remon, J.P.; Vervaet, C.; Baeyens,  
421 W.R.G. *J. Pharm. Biomed. Anal.* **2008**, *48*, 772-779
- 422 [3]. Campbell Roberts, S.N.; Williams, A.C.; Grimsey, I.M.; Booth, S.W. *J. Pharm.*  
423 *Biomed. Anal.* **2002**, *28*, 1135-1147
- 424 [4]. Al-Zoubi, N.; Koundourellis, J.E.; Malamataris, S. *J. Pharm. Biomed. Anal.* **2002**, *29*,  
425 459-467
- 426 [5]. Pratiwi, D.; Fawcett, J.P.; Gordon, K.C.; Rades, T. *Eur. J. Pharm. Biopharm.* **2002**, *54*,  
427 337-341
- 428 [6]. Strachan, C.J.; Pratiwi, D.; Gordon, K.C.; Rades, T. *J. Raman Spectrosc.* **2004**, *35*,  
429 347-352
- 430 [7]. De Beer, T.R.M.; Baeyens, W.R.G.; Ouyang, J.; Vervaet, C.; Remon, J. P. *Analyst*,  
431 **2006**, *131*, 1137-1144
- 432 [8]. Kogermann, K.; Aaltonen, J.; Strachan, C.J.; Pöllänen, K.; Heinämäki, J.; Yliruusi, J.;  
433 Rantanen, J. *J. Pharm. Sci.* **2008**, *97*, 4983-4999
- 434 [9]. Févotte, G. *Chem. Eng. Res. Des.* **2007**, *85(A7)*, 906-920
- 435 [10]. Caillet, A.; Puel, F.; Févotte, G. *Int. J. Pharm.* **2006**, *307*, 201-208
- 436 [11]. Hu, Y.R.; Liang, J.K.; Myerson, A.S.; Taylor, L.S. *Ind. Eng. Chem. Res.* **2005**, *44*,  
437 1233-1240
- 438 [12]. Ono, T.; Kramer, H.J.M.; ter Horst, J.H.; Jansens, P.J. *Cryst. Growth Des.* **2004**, *4*,

- 439 1161-1167
- 440 [13]. O'Sullivan, B.; Barrett, P.; Hsiao, G.; Carr, A.; Glennon, B. *Org. Proc. Res. Dev.* **2003**,
- 441 7, 977-982
- 442 [14]. Schöll, J.; Bonalumi, D.; Vicum, L.; Mazzotti, M.; Muller, M. *Cryst. Growth Des.*
- 443 **2006**, 6, 881-891
- 444 [15]. Starbuck, C.; Spartalis, A.; Wai, L.; Wang, J.; Fernandez, P.; Lindemann, C.M.; Zhou,
- 445 G.X.; Ge, Z. *Cryst. Growth Des.* **2002**, 2, 515-522
- 446 [16]. Wang, F.; Wachter, J.A.; Antosz, F.J.; Berglund, K.A. *Org. Proc. Res. Dev.* **2000**, 4,
- 447 391-395
- 448 [17]. Agarwal, P.; Berglund, K.A. *Cryst. Growth Des.* **2003**, 3, 941-946
- 449 [18]. Scheweinsberg, D.P.; West Y.D. *Spectrochimica Acta Part A*, **1997**, 53, 25-34
- 450 [19]. Aarnoutse, P.J.; Westerhuis, J.A. *Anal. Chem.* **2005**, 77, 1228-1236
- 451 [20]. Pelletier, M.J. *Appl. Spectrosc.* **2003**, 57, 20A-42A
- 452 [21]. Szostak, R.; Mazurek, S. *Journal of Molecular Structure*, **2004**, 704, 235-245
- 453 [22]. Wang, H.; Mann, C. K.; Vickers, T. J. *Appl. Spectrosc.* **2002**, 56, 1538-1544
- 454 [23]. Hu, Y.; Wikström, H.; Byrn, S. R.; Taylor, L. S. *Appl. Spectrosc.* **2006**, 60, 977-984
- 455 [24]. Pellow-Jarman, M.V.; Hendra, P.J.; Lehnert, R.J. *Vibrational Spectroscopy*, **1996**, 12,
- 456 257-261
- 457 [25]. Reis, M. M.; Araujo, P. H. H.; Sayer, C.; Giudici, R. *Polymer*, **2003**, 44, 6123-6128
- 458 [26]. Hamilton, P.; Littlejohn, D.; Nordon, A.; Sefcik, J.; Slavin, P.; Dallin, P.; Andrews, J.
- 459 *Analyst*, **2011**, 136, 2168-2174

460 [27]. Chen, Z.P.; Fevotte, G.; Caillet, A.; Littlejohn, D.; Morris, J. *Anal. Chem.* **2008**, *80*,  
461 6658-6665

462 [28]. Anderson, A. *The Raman effect, volume 2: Applications*, MerceL Dekker, Inc: New  
463 York, **1973**

464 [29]. Chen, Z.P.; Zhong, L.-J.; Nordon, A.; Littlejohn, D.; Holden, M.; Fazenda, M.;  
465 Harvey, L.; McNeil, B.; Faulkner, J.; Morris, J. *Anal. Chem.* **2011**, *83*, 2655-2659

466 [30]. Jin, J.W.; Chen, Z.P.; Li, L.M.; Steponavicius, R.; Thennadil, S.N.; Yang, J.; Yu, R.Q.  
467 *Anal. Chem.* **2012**, *84*, 320–326

468 [31]. Geladi, P.; MacDougall, D.; Martens, H. *Appl. Spectrosc.* **1985**, *39* (3), 491-500

469 [32]. Barnes, R.J.; Dhanoa, M.S.; Lister, S.J. *Appl. Spectrosc.*, **1989**, *43*, 772-777

470 [33]. Pedersen, D.; Martens, H.; Nielsen, J.; Engelsen, S. *Appl. Spectrosc.* **2002**, *56* (9),  
471 1206-1214

472

473

474

475

476

477

478

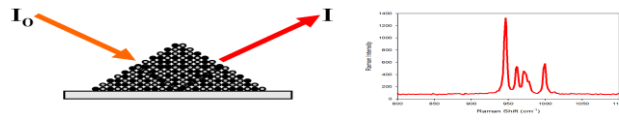
479

480

481

482

### For TOC only



483

